Zirconium under pressure: phase transitions and thermodynamics

2006 J. Phys.: Condens. Matter 18 1483

(http://iopscience.iop.org/0953-8984/18/5/001)

INSTITUTE OF PHYSICS PUBLISHING JOURNAL OF PHYSICS: CONDENSED MATTER

J. Phys.: Condens. Matter **18** (2006) 1483–1494 doi:10.1088/0953-8984/18/5/001

Zirconium under pressure: phase transitions and thermodynamics

I Schnell and R C Albers

Theoretical Division, Los Alamos National Laboratory, Los Alamos, NM 87545, USA

E-mail: ilan@viking.lanl.gov

Received 22 September 2005, in final form 19 December 2005
Published 17 January 2006
Online at stacks.iop.org/JPhysCM/18/1483

Abstract

In this paper, the full-potential linearized augmented plane-wave (LAPW) method within the generalized gradient approximation (GGA) was used to calculate the effect of hydrostatic pressure at zero temperature on the 4d transition metal zirconium. For the hexagonal close-packed (hcp), omega (ω), and body-centred cubic (bcc) structures the enthalpy, $H = E + pV$, was calculated as a function of pressure p. We obtained an ω to bcc transition pressure of 28.2 GPa. Temperature-dependent contributions were obtained from tight-binding calculations of the phonons in the quasiharmonic approximation and were used to calculate the Gibbs free energy as a function of both temperature T and pressure for these three structures. From the comparison of these free energies the phase boundaries were calculated in the T–p phase diagram, and compared to the experimentally determined boundaries. We discuss the importance of anharmonicity for understanding the material properties of zirconium, and limitations of quasiharmonic phonon theories for predicting phase transformations.

1. Introduction

Density-functional theory (DFT) calculations based on the generalized gradient approximation (GGA) [1, 2] have proven to be an effective tool for studying the properties of many systems at zero temperature, ranging from bulk materials to clusters and surfaces. With the availability of increasingly powerful computers and efficient algorithms, it is now possible to perform calculations for reasonably large systems. Despite these advances, the application of *ab initio* methods to the study of finite-temperature thermodynamic effects such as thermal expansion and phase diagrams remains challenging, since such effects involve lattice contributions to the free energy that can be difficult to evaluate, especially if anharmonic contributions are important. In this paper we use tight-binding methods to extend first-principles approaches in order to calculate the free energy and phase diagram of a complex transition-metal material, zirconium.

The thermodynamic properties of zirconium have been the subject of many experimental [3–9] and theoretical [1, 10–13] studies. At room temperature and ambient pressure, the stable crystalline state of this early 4d transition metal is a hexagonal close-packed (hcp) structure (the α phase). When the temperature is raised, at zero pressure, Zr transforms martensitically into the body-centred cubic (bcc) structure (the β phase) at 1136 K, and then eventually melts out of the bcc phase. When the pressure is increased at room temperature, a martensitic phase transformation into the omega structure (ω phase) is observed between 3.3 and 6.7 GPa [14]. At even higher pressures, 30–35 GPa, Zr exhibits a martensitic transformation into the bcc structure [3–6].

This paper is organized as follows. In section 2, we focus on the zero-temperature transitions of Zr under pressure. To this end, we have calculated the enthalpy has a function of pressure for the bcc, hcp, and ω structures. For the hcp and ω structure, we have minimized the energy at each volume by varying the c/a ratio. In section 3, we have added temperature-dependent contributions and calculated the Gibbs free energy as a function of both temperature and pressure for these three structures using phonons obtained by the tight-binding approach within the quasiharmonic approximation. Comparison of these free energies enables us to calculate phase boundaries in the $T-p$ phase diagram. We finish the paper with a summary and discussion in section 4.

2. Zero-temperature transitions

2.1. Details of the calculation

We have used the WIEN2k full-potential LAPW package [15] to calculate the zero-temperature total energies for the three structures (bcc, hcp, and ω) considered. The GGA [2] potential was used to include the effects of exchange and correlation. Aiming at high precision, we used a plane-wave cutoff of $RK_{\max} = 9$, a largest vector in the charge density Fourier expansion of $G_{\max} = 20/a_0$ (a_0 is one Bohr radius, $\approx$0.529 Å), and a criterion of 0.01 mRyd for energy convergence. The muffin-tin radius was set to $2.0a_0$ in all calculations. We carefully checked the convergence in terms of k-points: for the bcc structures, we show in figure 1 the convergence as a function of volume. Much to our surprise, the convergence is far better at experimental volume (23.34 Å) than for the high pressure (small volume) regime. For the other two structures (hcp and ω), we tested the convergence at ambient pressure and in the high pressure regime. In order to converge the total energy below 0.1 mRyd/atom, we chose 30 000 k-points in the full Brillouin zone (BZ) for the bcc structure, 7500 k-points in the full BZ for the hcp structure, and 2000 k-points in the full BZ for the ω structure, corresponding to 816, 427, and 128 k-points in the irreducible wedge of the BZ, respectively.

For the bcc structure, we calculated the total energy E at six volumes V and fitted our energy–volume data points with the Rose equation of state [16].

For the hcp and the ω structures we optimized the c/a ratio (as a function of volume or pressure) by first determining the c/a range for each structure and then calculating the Rose equation of state for five (hcp) or four (ω) fixed c/a ratios (in the same manner as done for the bcc structure). Using these equations of state, we can pick any fixed volume V and fit a parabola to the total energy as a function of c/a. The minimum of this parabola corresponds to the c/a ratio and the total energy E (for volume V). In this way we can obtain c/a and E as a function of volume. Finally, we fit $E(V)$ to our equations of state, and from this we can also determine the functional dependence of c/a on pressure through its volume, i.e., $c/a(p) = c/a(V(p))$. Finally, we also calculate the enthalpy $H = E + pV$ for the three structures as a function of pressure p.

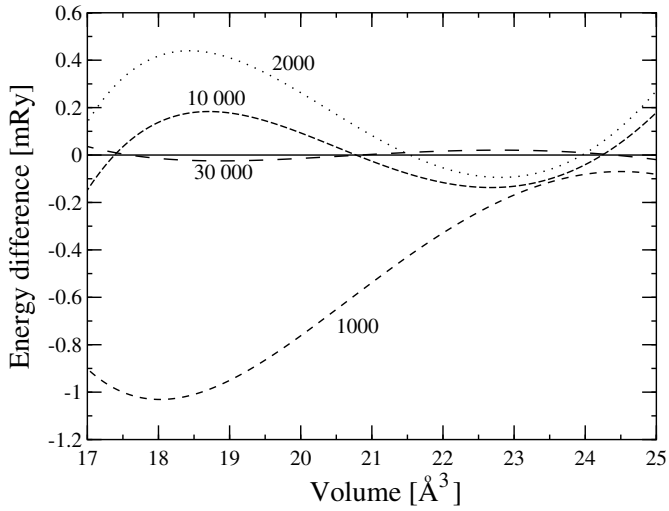

Figure 1. DFT-GGA: total energy difference versus volume for the bcc structure for different number of k-points (with respect to the total energy calculated with 100 000 k-points).

We should note that the root-mean-square errors of both the equations of state fits and the parabola fits were found to be well below 0.1 mRyd/atom, such that 0.1 mRyd/atom remains our error estimate for total energies.

2.2. Results

Figure 2 shows the enthalpy $H = E + pV$ as a function of pressure p (with respect to the enthalpy of the bcc structure) for the three structures considered (bcc, hcp, and ω). At zero pressure, we found the ω structure to have the lowest enthalpy, and to be 0.15 mRyd/atom lower than for the hcp structure. We found the same total energy differences between these two structures at the experimental volume. However, Jomard *et al* [11] found the opposite. In their calculations the hcp structure was 0.25 mRyd/atom lower than the ω structure at the experimental volume, using the PW91 GGA functional [17] at a level of convergence of 0.15 mRyd/atom. Nonetheless, all of these energy differences are very close to the level of convergence of first-principles band-structure calculations, and, for practical purposes, one should probably consider both structures to be effectively degenerate.

At 21.0 GPa we found the enthalpy of hcp to cross that of the bcc; however, the enthalpy of the ω structure is still lower than that of the other two.

Of more interest is the crossing of the enthalpy of the ω structure with the enthalpy of the bcc structure, which occurs at 28.2 ± 0.4 GPa. The estimated error was determined by shifting the energy of one of these structures by 0.1 mRyd/atom (note that we converged all total energies below this value) in order to see the effect on the transition pressure, which changed by about 0.4 GPa. Our calculated transition pressure is in good agreement with experimental results from Xia *et al* [3, 4], who found the transition pressure to be about 30–35 GPa through diamond-anvil experiments. It is also in good agreement with the GGA result of 29.1 GPa [12], although the c/a ratio of the ω structure was assumed constant in these calculations (see below).

We have summarized the various experimental and theoretical results in table 1. Due to the variety of different LDA results found in the literature for the $\omega \rightarrow$ bcc transition pressure, we have calculated this pressure using the LDA [18] to include the effects of exchange and

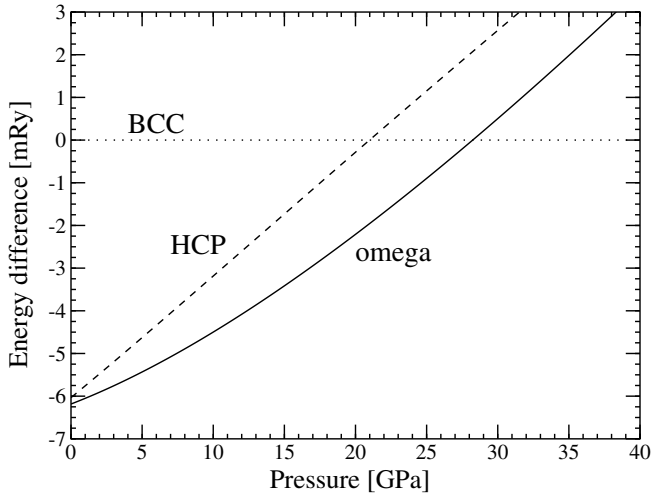

Figure 2. DFT-GGA: enthalpy H of the three structures with respect to the enthalpy of the bcc structure.

Table 1. The $\omega \rightarrow$ bcc transition pressure from various references. 'A' refers to this work. The experimental results are at room temperature.

LDA		GGA		Expt.	
p (GPa)	Reference	p (GPa)	Reference	p (GPa)	Reference
5.0	[10]	35.4	[11]	30 ± 2	[3]
48.3	[13]	29.1	[12]	35 ± 3	[4]
11.2	[11]	28.2 ± 0.4	A	31	[5]
17.8	[12]			33	[6]
16.2 ± 0.3	A				

correlation. Except for using the LDA (instead of the GGA), all details of the calculation are the same as described above. From the LDA we find the $\omega \rightarrow$ bcc transition pressure to be at 16.2 ± 0.3 GPa.

Figure 3 shows the pressure dependence of the c/a ratio of the hcp and the ω structure (GGA again). At zero pressure we find $c/a = 1.591$ for the hcp structure and $c/a = 0.624\,55$ for the ω structure. These results compare very well with experimental values, which are 1.593 for hcp [19] and 0.625 ± 0.002 for ω [3].

At the $\omega \rightarrow$ bcc transition pressure (28.2 GPa), we find $c/a = 0.622\,75$ for the ω structure which is only 0.3% smaller than the c/a ratio at zero pressure. For the transition pressure, the difference of the total energy of the ω structure at these two c/a ratios is only about 5 μRyd—far smaller than our error estimate. Therefore it is justified (as done in [12]) to assume c/a constant for the ω structure. However, for the hcp phase we find c/a increasing by about 7% when increasing the pressure from zero to 40 GPa. Jona and Marcus [10] have also calculated the c/a as a function of pressure from the LDA. They find the same trend, i.e., the c/a for the hcp structure increases with pressure and c/a for the ω structure decreases with pressure. However, over the range of pressure from 0 to 20 GPa they see about a 3% change in the c/a ratio for the ω structure, which is more than one magnitude larger than our result.

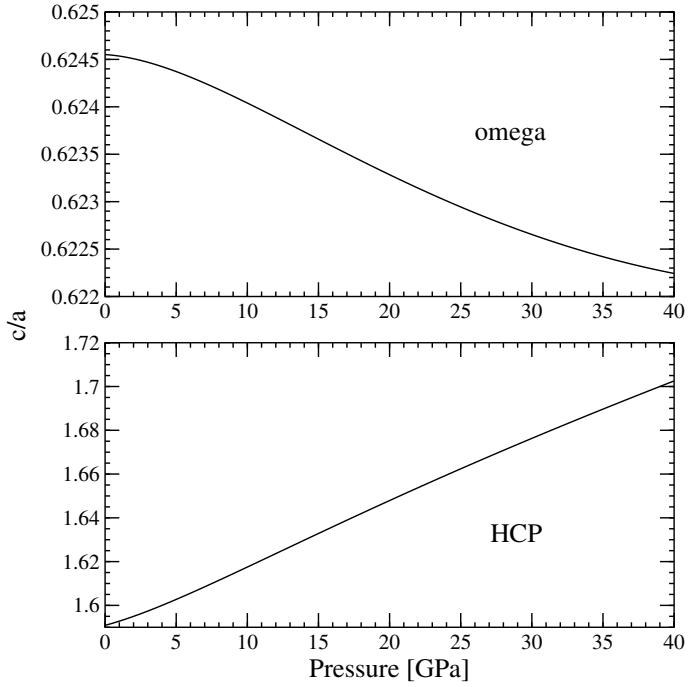

Figure 3. DFT-GGA: c/a ratio as a function of pressure of the ω and the hcp structures.

3. Finite-temperature treatment

To calculate the temperature–pressure phase diagram, i.e., the temperature dependence of the phase transitions caused by pressure, a knowledge of the Gibbs free energy $G(T, p)$ is required. We have used the NRL tight-binding (TB) approach [20] to calculate the zero-temperature phonons within the quasiharmonic approximation for the three structures. Knowledge of these phonons, as well as the electronic density of states, makes it possible to calculate the temperature-dependent contributions to the free energy.

3.1. Tight-binding approach

The NRL tight-binding approach [20] is designed to reproduce *ab initio* DFT calculations by fitting the model parameters to DFT band structures and total energies. Being a parameterized version of the DFT calculations, the method is computationally orders of magnitude faster than DFT itself.

The total DFT energy is given by ($i = \{\mathbf{k}, n\}$)

$$E[n] = \sum_i f(\epsilon_i - \mu)\epsilon_i + F[n], \qquad f(z) = \frac{1}{1 + \mathrm{e}^{\beta z}}, \tag{1}$$

that is, a sum over the energy eigenvalues ϵ_i (weighted by the Fermi function f) plus a remaining density functional $F[n]$ which contains (i) the ion–ion interaction energy, (ii) parts of the Hartree and exchange energy not yet included in the sum, and (iii) corrections for double counting. In the NRL-TB model, the Kohn–Sham potential (and hence the eigenvalues ϵ_i) are shifted by $V_0 = F[n]/N_e$, such that $E[n] = \sum_i f(\epsilon_i' - \mu')\epsilon_i'$. The shifted ϵ_i' are considered functions of only the crystal structure and the volume. The tight-binding method reproduces ϵ_i'

over a wide range of structures and volumes and solves the shifted total energy problem. For the nonorthogonal tight-binding model we use a basis consisting of s, p, and d orbitals. This models requires 73 parameters of which 60 are used to describe the intersite matrix elements of the Hamiltonian

$$h_{\ell\ell' m}(r) = (a_{\ell\ell' m} + b_{\ell\ell' m} r) \exp(-c^2_{\ell\ell' m} r) f_c(r), \tag{2}$$

and overlap matrix

$$s_{\ell\ell' m}(r) = (a'_{\ell\ell' m} + b'_{\ell\ell' m} r) \exp(-c'^2_{\ell\ell' m} r) f_c(r), \tag{3}$$

where $f_c(r) = 1/(1 + e^{2(r-r_0)})$ is a function which ensures a smooth cutoff at large distances (we use $r_0 = 17.0$ Bohr). The on-site Hamilton matrix elements are described by

$$e_\alpha = e^0_\alpha + e^1_\alpha \rho^{2/3} + e^2_\alpha \rho^{4/3} + e^3_\alpha \rho^2 \tag{4}$$

where α denotes the ℓ character of the orbital, i.e., s, p, and d, and ρ is a measure of the valence electron density, given by

$$\rho = \sum_{i \neq j} \exp(-\lambda^2 r_{ij}) f_c(r_{ij}). \tag{5}$$

The accuracy and transferability of the method depends on the determination of these 73 parameters.

The database used for fitting the tight-binding parameters of zirconium consists of energy bands and total energies calculated using the WIEN2k full-potential LAPW package [15]. Again, the GGA [2] potential was used to include the effects of exchange and correlation. To fit the 73 parameters to the DFT database, we use a standard nonlinear least-squares algorithm [21], the Levenberg–Marquardt method. For the cubic structures, the symmetry of special **k**-points in the first Brillouin zone is taken into account [22]. The database consists of DFT calculations for bcc, fcc, simple cubic, hcp, diamond, and ω structures at nine volumes around the experimental equilibrium volume, ranging from 16 to 30 Å.

Using this database, we have created a tight-binding fit, in which we have included total DFT energies (with weights between 1000 and 5000 larger than the weights of the individual energy eigenvalues) in the fitting procedure. Our root-mean-square error for the total-energies fit (for the various structures and volumes) was about 2.5 mRyd/atom.

3.2. Phonons

In order to calculate the phonons, we evaluated the force constants from the tight-binding model by using the direct-force method [23], which relies on calculating the forces on all atoms (l, k), i.e., the kth atom in lth cell, in the supercell in which one atom $(0, k')$ has been displaced from its equilibrium position. In the quasiharmonic approximation, the force constants are given by

$$\phi_{\alpha\beta}(0k', lk) = -\frac{\partial F_\beta(l, k)}{\partial u_\alpha(0, k')} \approx -\frac{F_\beta(l, k)}{u_\alpha(0, k')}, \tag{6}$$

i.e., the ratio of the negative force on atom (l, k) in the β direction to the displacement of atom $(0, k')$ in the α direction. In the tight-binding model, the actual calculation of the forces in equation (6) is achieved by evaluating analytic derivatives of the Hamiltonian and overlap matrix elements and the on-site terms [24]. Once the forces constants have been calculated, the phonons are evaluated by diagonalizing the dynamical matrix

$$M_{\alpha\beta}(\mathbf{q}, kk') = \sum_{l'} \phi_{\alpha\beta}(0k, l'k') \exp\left\{i\mathbf{q} \cdot [\mathbf{x}(l', k') - \mathbf{x}(0, k)]\right\}, \tag{7}$$

where $\mathbf{q}$ is the wavevector and $\mathbf{x}(l, k)$ is the atom position. However, if the forces do not vanish inside the supercell, we introduce errors due to (super) cell–cell interactions. The supercell,

consisting of replicas of the primitive or conventional unit cell, in general does not have the crystal symmetry. Therefore, cell–cell interactions will contribute force constants which violate the symmetry rules of the force constants. Let S_m be a space group element, **S** its proper or improper rotation and **v** its translation; that is,

$$S_m\mathbf{x}(l,k) = \mathbf{x}(L,K) = \mathbf{S}_m\mathbf{x}(l,k) + \mathbf{v}_m. \tag{8}$$

Then

$$\phi_{\alpha\beta}(lk,l'k') = \mathbf{S}_m\phi_{\alpha\beta}(lk,l'k')\mathbf{S}_m^T, \tag{9}$$

where ϕ is a $3\times$ 3 matrix with elements $\phi_{\alpha\beta}$ (see [25]). Since equation (9) will no longer hold when cell–cell interactions are present, it is necessary to restore this symmetry in order for the phonons to have the correct symmetry, i.e., the eigenvalues of equation (7) are unchanged by $\mathbf{q} \to \mathbf{Sq}$. We achieve this by applying all symmetry operations, and then averaging over these within equation (9). This means replacing

$$\phi_{\alpha\beta}(0k,l'k')\exp\left\{i\mathbf{q}\cdot[\mathbf{x}(l',k') - \mathbf{x}(0,k)]\right\}, \tag{10}$$

in equation (7) by

$$\frac{1}{N}\sum_{m=1}^{N}\mathbf{S}_m\phi_{\alpha\beta}(0k,l'k')\mathbf{S}_m^T\exp\left\{i\mathbf{q}\cdot S_m[\mathbf{x}(l',k') - \mathbf{x}(0,k)]\right\}, \tag{11}$$

where N is the number of space group elements. Using this scheme, we have calculated the phonon energies from force constants evaluated from $3\times3\times3$ supercells for the three structures for 12 different volumes corresponding to pressures ranging from -5 to 40 GPa. Figure 4 shows a comparison of the phonons calculated at ambient pressure with experimental phonon data from neutron scattering [9]. Although the discrepancies between theory and experiment, which are probably mainly due to tiny errors in the tight-binding fits (of the order of fractions of mRyd), are larger than we would ideally like, the level of accuracy is reasonably adequate for thermodynamic properties, since such calculations average over the entire phonon spectra.

3.3. Melting criteria

From the phonon density of states, we have calculated the root-mean-square displacement of each atom from its equilibrium site in terms of the mean radius (Wigner–Seitz radius S), as a function of temperature, i.e., $x = \sqrt{\langle u^2\rangle}/S$. The quantity $\langle u^2\rangle$ can be evaluated by expressing u in terms is creation and annihilation operators, and we find

$$\langle u^2\rangle = \int \frac{\hbar}{M\omega}\left(1 + \frac{2}{\exp(\hbar\omega/k_BT) - 1}\right)g(\omega)\,d\omega, \tag{12}$$

where M is the mass of one atom. Figure 5 shows x calculated from the hcp phonon density of states at ambient conditions. The zero-temperature motion is about 6% of the Wigner–Seitz radius. The Lindemann melting criterion suggests that the solid will melt when x approaches some standard value x_m which seems to be in the range of 0.2–0.25 for most solids [26]. According to this criterion, neglecting the fact that Zr melts in its bcc phase at ambient pressure, the melting should occur between 625 and 980 K, which is much lower that the experimentally observed [14] melting temperature T_m of 2128 K. This discrepancy suggest a large temperature dependence of the phonons, which is in fact observed experimentally [9]. Our quasiharmonic phonons are calculated at zero temperature and have no temperature dependence.

The Lindemann melting formula [27], which can be written as

$$x_m^2 M k_B \Theta^2 S^2 = 9\hbar^2 T_m, \tag{13}$$

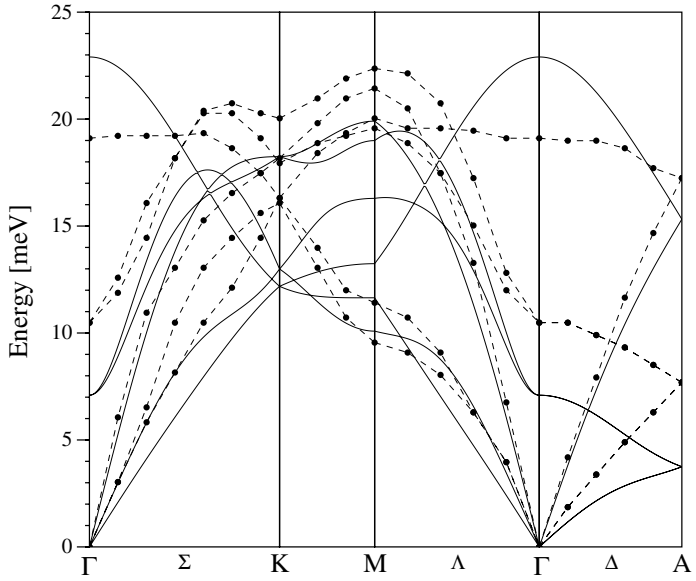

Figure 4. The hcp phonon energy band structure. The solid lines show the phonon frequencies from our tight-binding fit, the dot–dashed lines show the experimental phonon frequencies from neutron scattering at 295 K [9].

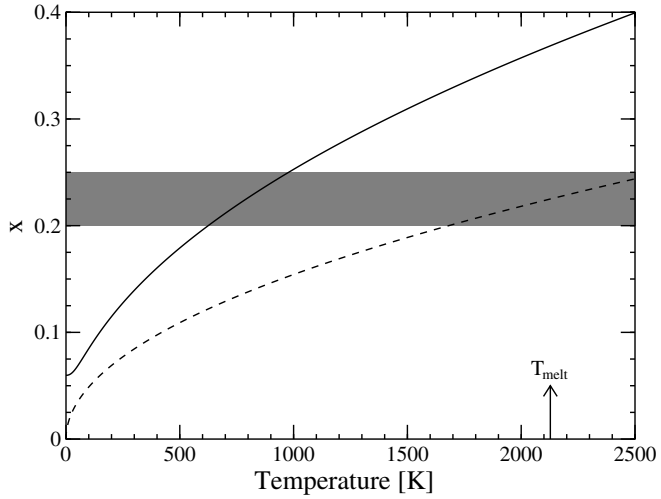

Figure 5. Root-mean-square displacement divided by the Wigner–Seitz radius S, i.e. $x = \sqrt{\langle u^2 \rangle}/S$. The solid line shows x as calculated from the phonon density of states, and the dashed line shows $x = \sqrt{9\hbar^2 T/Mk_B\Theta^2}/S$ with a Debye temperature of $\Theta = 253$ K, and $S = 3.35$ Bohr. The shaded region indicates the range of x where solids typically melt. We have also indicated the experimental melting temperature.

may be used to estimate the Debye temperature Θ from the melting temperature. Using $x_m = 0.225$ and $T_m = 2128$ K in equation (13) one obtains $\Theta = 253$ K, which is in good agreement with other experimental data [28]. Using this Debye temperature, we have also plotted x from equation (13) in figure 5.

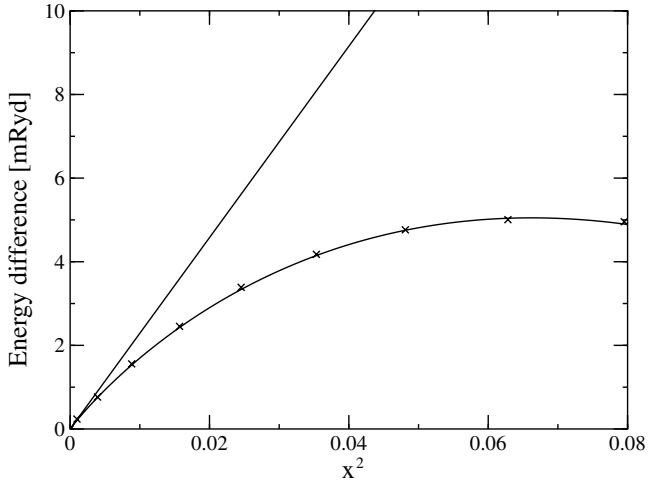

Figure 6. Energy of the transverse optical phonon at the Γ-point as a function of displacement squared in the scaled units of $x = u/S$ as calculated by DFT (Wien2k). We fit the values to an equation of the form $\Delta E = ax^2 + bx^3$. This is the curved line in the figure and it passes through the calculated values indicated by small crosses. The straight line is a plot of the first term to the fit and corresponds to harmonic behaviour. The coefficient a gives a calculated phonon frequency of 9.54 meV; the experimental value [9] at room temperature is 10.5 meV. Note that the curve already begins to strongly deviate from the expected linear harmonic behaviour by $x^2 = 0.01$ or $x = 0.1$.

Zirconium has very strong anharmonicities, which we believe is a major cause of many of the anomalies seen in physical properties. The phonons have a well-known temperature dependence [9]. Theoretical papers attempting to explain the mechanism for the bcc to ω transformation have focused on the L(2/3, 2/3, 2/3) bcc phonon of Zr, which softens as a function of temperature and is a precursor to the ω transformation. See, for example, [29] and papers cited in [1] and [30]. A typical example of the anharmonicity of Zr is the restoring force for the frozen L(2/3, 2/3, 2/3) phonon as a function of displacement that is shown in figure 4 of [29], which oscillates in sign as the displacements become larger. Similarly, in figure 6 we show the dependence of the frozen phonon energy for the transverse optical phonon at the Γ-point as a function of displacement squared as calculated by DFT (Wien2k). Strong deviations from harmonic behaviour already occur at an x as small as 0.1. This corresponds to the average displacement of Zr at a temperature between 100 and 400 K (depending on the model used for the mean displacement; see figure 5). All of these calculations indicate how quickly Zr becomes anharmonic as a function of displacement for any type of phonon mode. In our phonon calculations we used a rather small value of displacement, corresponding to a $u = 0.03$ Bohr (or $x = 0.009$), in order to be sure that our phonons were in the harmonic limit and were independent of displacement. Clearly, these types of anharmonicities can affect the phase diagram at higher temperatures.

3.4. Free energy and phase diagram

We are now in a position to calculate the free energy in the quasiharmonic approximation [31]. In this approximation, the ionic contribution to the free energy depends on the volume-dependent phonon density of states, $g(\omega, V)$, through the zero-point energy

$$U_{\text{zero}}(T, V) = \int \hbar\omega \left[\frac{1}{\exp(\hbar\omega/k_{\text{B}}T) - 1} + \frac{1}{2} \right] g(\omega, V)\, \mathrm{d}\omega \tag{14}$$

and the quasiharmonic free energy [32]

$$F_{\mathrm{H}}(T, V) = k_{\mathrm{B}}T \int \ln\left[1 - \exp(-\hbar\omega/k_{\mathrm{B}}T)\right] g(\omega, V)\, \mathrm{d}\omega. \tag{15}$$

The electronic contribution, which we found to be one order of magnitude smaller than the ionic contribution, depends on the volume-dependent electronic density of states, $n_{\mathrm{el}}(E, V)$, and is given by [32]

$$F_{\mathrm{el}}(T, V) = k_{\mathrm{B}}T \int \left[f \ln f + (1 - f)\ln(1 - f)\right] n_{\mathrm{el}}(E, V)\, \mathrm{d}E. \tag{16}$$

Adding these contributions to the zero-temperature internal energy, we have evaluated the Helmholtz free energy F as a function of temperature and volume (within the quasiharmonic approximation).

In order to calculate the phase digram, it is necessary to use T and p as independent variables, instead of T and V. Using [33]

$$\left(\frac{\partial F}{\partial V}\right)_T = -p, \tag{17}$$

we can calculate the volume V corresponding to a given pressure p for a given temperature T. This enables us to evaluate the Gibbs free energy

$$G(T, p) = F(T, V) + pV \tag{18}$$

for the three crystal structures.

Comparison of these energies as a function of pressure and temperature allows us to identify the transformation lines. It should be pointed out that this approach is extremely demanding, since very small errors in the Gibbs free energies can drastically change the phase transformation lines. Figure 7 shows a comparison of the predicted phase boundaries with experimental results. Note that not all phase boundaries can be predicted with our model, because the quasiharmonic phonons in some volume ranges for the different phases are unstable, i.e., some phonon frequencies are imaginary. In particular, the hcp phase becomes unstable at high pressures, whereas the bcc phase becomes unstable at low pressures. This is a generic problem when calculating any phase diagram from quasiharmonic phonons (whether calculating the phonons from tight-binding or LDA/GGA first-principles band-structure methods). High-temperature phases are often stabilized by temperature-dependent phonons and theories based on zero-temperature phonons will simply prove inadequate. To fix this problem will require either self-consistent phonon theories or possibly some form of molecular dynamics that uses electronic structure theory to calculate the forces between the atoms in a large supercell. Given how difficult phase diagrams are to calculate, the agreement in figure 7 is quite reasonable.

To plot the experimental $\omega \rightarrow$ bcc transition line we have indicated the range of experimental values reported in the literature (see table 1). Our calculated value is at the low end of these values. The most likely cause for this discrepancy is because small amounts of impurities can block the martensitic transitions in these types of metals (see, for example, the case for the related material Ti [34]), and cause the transition pressure to move to higher pressures. Since our zero-temperature transition pressure is based on high-quality first-principles approaches and agrees well with similar calculations by Grad *et al* [12], we feel that our predicted transition pressure is likely to be close to the true equilibrium value.

Our zero-temperature band-structure results predict that the ω phase has a slightly lower enthalpy than hcp phase (the room-temperature equilibrium phase); however, if zero-point motion effects are added to the enthalpy, the situation reverses and we find that the hcp phase

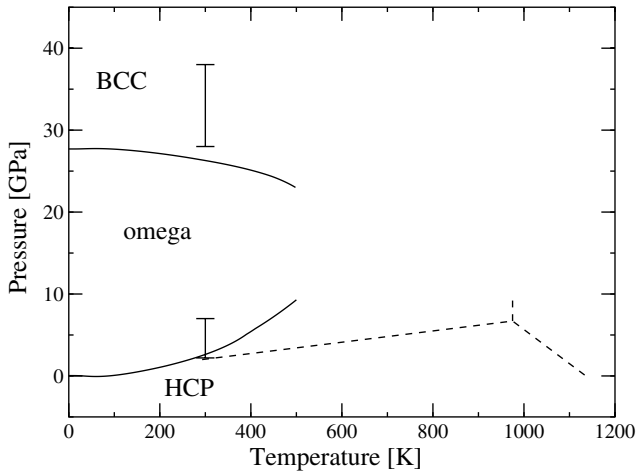

Figure 7. Predicted phase diagram. The solid lines show the predicted phase boundaries from our tight-binding fit, and the dashed lines show some of the experimental results. The dashed lines are from [14]. The bar at room temperature for the bcc to ω transition represents the range of experimental values for this transition (see table 1) and includes experimental error bars. The bar at room temperature for the hcp to ω transition represents the range of experimental values for this transition; see the range of values summarized in [35].

is the more stable zero-temperature phase for Zr. In fact, if we carefully plot our predicted phase boundary line as a function of temperature, we find that the hcp and ω phases go through a single oscillation in stability with transition pressures of the order of 0.1 GPa. This is an indication that, within the accuracy of our calculations, for all temperatures below 100 K both phases have almost identical free energies and we cannot distinguish which phase is more stable. For all temperatures above 100 K, we find that the hcp phase is more stable than the ω phase at zero pressure (cf figure 7). At higher temperatures, we find that the predicted pressure for the transition tends to curve above the experimental values. We believe that this is caused by the optical Γ-point phonons becoming unstable in the hcp phase in our tight-binding calculations. DFT-GGA calculations for these zone-centre optical phonons did not have these instabilities.

4. Summary

In this work, we have investigated the phase transitions of solid zirconium at zero and finite temperatures. From the GGA, we have found the $\omega \rightarrow$ bcc transition pressure at $T = 0$ to be 28.2 ± 0.4 GPa, which is only a little lower than the experimental results that range between 28 and 38 GPa at room temperature. It is likely that impurity effects cause an elevated experimental transition pressure. The calculated c/a ratios for the hcp and ω structures at zero pressure are in very good agreement with experiment.

In order to treat finite-temperature effects, we included temperature-dependent contributions and calculated the Gibbs free energy. For the relevant pressure range for the three structures, we have calculated phonons using the tight-binding approach within the quasiharmonic approximation. Phonons for the hcp structure at ambient pressure compare reasonably well with experiment. The theoretically predicted phonons were used to calculate phase boundaries in the T–p phase diagram. At high temperatures, our calculations are likely to have errors, since we are using zero-temperature quasiharmonic phonons to calculate the thermodynamic free energies. According to experiment [9], the phonons have a strong temperature dependence at high temperatures.

We are only able to calculate pieces of the phase boundaries due to the instability of quasiharmonic phonons for the different phases, which often are only stable for a limited range of lattice constants. The experimental phonons at finite temperature in Zr are stabilized by the strong anharmonic behaviour of the atomic forces. Future work will need to find some way to include these strong anharmonicities in order to extend the pieces of the phase boundaries that can be calculated and to improve the agreement with experiment at higher temperatures.

Acknowledgments

This work was supported by the Department of Energy under contract W-7405-ENG-36. This research used resources of the National Energy Research Scientific Computing Center, which is supported by the Office of Science of the US Department of Energy under Contract No. DE-AC03-76SF00098.

References

[1] Kuebler J and Eyert V 1992 Electronic structure calculations *Electronic and Magnetic Properties of Metals and Ceramics* ed K H J Buschow (Weinheim: VCH) pp 1–145
Kuebler J and Eyert V 1992 *Materials Science and Technology* vol 3A, ed R W Cahn, P Haasen and E J Kramer (Weinheim: VCH) pp 1991–6
[2] Perdew J P, Burke K and Ernzerhof M 1996 *Phys. Rev. Lett.* **77** 3865
[3] Xia H, Duclos S J, Ruoff A L and Vohra Y K 1990 *Phys. Rev. Lett.* **64** 204
[4] Xia H, Ruoff A L and Vohra Y K 1991 *Phys. Rev.* B **44** 10374
[5] Akahama Y, Kobayashi M and Kawamura H 1990 *J. Phys. Soc. Japan* **59** 3843
[6] Akahama Y, Kobayashi M and Kawamura H 1991 *J. Phys. Soc. Japan* **60** 3211
[7] Fisher E S and Renken C J 1964 *Phys. Rev.* **135** A482
[8] Collings E W and Ho J C 1971 *Phys. Rev.* B **4** 349
[9] Stassis C, Zarestky J, Arch D, McMasters O D and Harmon B N 1978 *Phys. Rev.* B **18** 2632
[10] Jona F and Marcus P M 2003 *J. Phys.: Condens. Matter* **15** 5009
[11] Jomard G, Magaud L and Pasturel A 1998 *Phil. Mag.* B **77** 67
[12] Grad G B, Blaha P, Luitz J, Schwarz K, Guillermet A F and Sferco S J 2000 *Phys. Rev.* B **62** 12743
[13] Ahuja R, Wills J M, Johansson B and Eriksson O 1993 *Phys. Rev.* B **48** 16269
[14] Young D A 1991 *Phase Diagrams of the Elements* (Berkeley: University of California)
[15] Blaha P, Schwarz K, Madsen G K H, Kvasnicka D and Luitz J 2001 WIEN2k *An Augmented Plane Wave + Local Orbitals Program for Calculating Crystal Properties* (Karlheinz Schwarz, Techn. Universität Wien, Austria) ISBN 3-9501031-1-2
[16] Rose J, Smith J, Guinea F and Ferrante J 1984 *Phys. Rev.* B **29** 2963
[17] Perdew J P and Wang Y 1986 *Phys. Rev.* B **33** 8800
[18] Perdew J P and Wang Y 1992 *Phys. Rev.* B **45** 13244
[19] Donohue J 1974 *The Structure of the Elements* (New York: Wiley) chapter 6
[20] Mehl M J and Papaconstantopoulos D A 1996 *Phys. Rev.* B **54** 4519
[21] Dennis J E Jr, Gay D M and Welsch R E 1981 *ACM Trans. Math. Softw.* **7** 348
[22] Jones M D and Albers R C 2002 *Phys. Rev.* B **66** 134105
[23] Ackland G J, Warren M C and Clark S J 1997 *J. Phys.: Condens. Matter* **9** 7861
[24] Cohen R E, Stixrude L and Wassermann E 1997 *Phys. Rev.* B **56** 8575
[25] Venkataraman G, Feldkamp L A and Sahni V C 1975 *Dynamics of Perfect Crystals* (Cambridge, MA: MIT Press)
[26] Ziman J M 1964 *Principles of the Theory of Solids* (Cambridge: Cambridge University Press)
[27] Lindemann F A 1910 *Z. Phys.* **11** 609
[28] Chen Q and Sundman B 2001 *Acta Mater.* **49** 947
[29] Ho K M, Fu C L and Harmon B N 1983 *Phys. Rev.* B **28** 6687
[30] Ho K M and Harmon B N 1990 *Mater. Sci. Eng.* A **127** 155
[31] Maradudin A A, Montroll E W, Weiss G H and Ipatova I P 1971 *Theory of Lattice Dynamics in the Harmonic Approximation* 2nd edn (New York: Academic)
[32] Pathria R K 1972 *Statistical Mechanics* (Oxford: Pergamon)
[33] Reif F 1965 *Fundamentals of Statistical and Thermal Physics* (Singapore: McGraw-Hill)
[34] Hennig R G, Trinkle D R, Bouchet J, Srivastava S G, Albers R C and Wilkins J W 2005 *Nat. Mater.* **4** 129
[35] Olijnyk H and Jephcoat A P 1997 *Phys. Rev.* B **56** 10751